Eur. Phys. J. Plus (2015) **130**: 70
DOI 10.1140/epjp/i2015-15070-0

THE EUROPEAN PHYSICAL JOURNAL PLUS

Review

The status of the macromolecular crystallography beamlines at the European Synchrotron Radiation Facility*

Christoph Mueller-Dieckmann[1], Matthew W. Bowler[2,3], Philippe Carpentier[1], David Flot[1], Andrew A. McCarthy[2,3], Max H. Nanao[2,3], Didier Nurizzo[1], Petra Pernot[1], Alexander Popov[1], Adam Round[2,3], Antoine Royant[1,4], Daniele de Sanctis[1], David von Stetten[1], and Gordon A. Leonard[1,a]

[1] Structural Biology Group, European Synchrotron Radiation Facility, CS 40220, 38043, Grenoble Cedex 9, France
[2] EMBL Grenoble Outstation, 71 avenue des Martyrs, CS 90181, 38042, Grenoble Cedex 9, France
[3] Unit for Virus Host-Cell Interactions, University of Grenoble Alpes-EMBL-CNRS, 71 Avenue des Martyrs, 38042, Grenoble Cedex 9, France
[4] Institut de Biologie Structurale, 71 avenue des Martyrs, CS 10090, 38044, Grenoble Cedex 9, France

Received: 20 February 2015
Published online: 15 April 2015 –

Abstract. The European Synchrotron Radiation Facility (ESRF) is the oldest and most powerful 3rd generation synchrotron in Europe, providing X-rays to more than 40 experimental stations welcoming several thousand researchers per year. A major success story has been the ESRF's facilities for macromolecular crystallography (MX). These are grouped around 3 straight sections: On ID23 canted undulators accommodate ID23-1, a mini-focus tuneable energy end station and ID23-2, the world's first micro-focus beamline dedicated to MX; ID29 houses a single, mini-focus, tuneable energy end station; ID30 will provide three end stations for MX due in operation from mid-2014 to early 2015. Here, one branch of a canted X-ray source feeds two fixed-energy end stations (MASSIF-1, MASSIF-3). The second feeds ID30B, a variable focus, tuneable energy beamline. MASSIF-1 is optimised for automatic high-throughput experiments requiring a relatively large beam size at the sample position, MASSIF-3 is a high-intensity, micro-focus facility designed to complement ID23-2. All end stations are highly automated, equipped with sample mounting robots and large area, fast-readout photon-counting detectors. Experiment control and tracking is achieved via a combination of the MXCuBE2 graphical user interface and the ISPyB database, the former allowing user-friendly control of all beamline components, the latter providing data tracking before, after and during experiments.

1 Introduction

The European Synchrotron Radiation Facility[1] (ESRF), Europe's first 3rd generation synchrotron source is located in Grenoble, France. Open for experiments since 1994, the ESRF is currently funded by a consortium comprising 13 Member Countries and 8 Scientific Associates. The ESRF storage ring, 844 metres in circumference, operates at an electron energy of 6 GeV with maximum current depending on the filling mode used. The characteristics of the most common filling mode, "7/8+1" operation[2], are a maximum current of 200 mA, horizontal and vertical electron beam emittances of 4 nm and 5 pm, respectively, an average lifetime greater than 50 hours and refill of the storage ring every 12 hours.

The ESRF has a long history in providing facilities for the practice of macromolecular crystallography (MX). The first phase of beamline construction at ESRF included the undulator beamlines ID09 (mainly dedicated to Laue diffraction experiments but which allocated part of its beam time to the MX community for single wavelength data collection), ID02 and ID13 [1,2] on which part of the beam time available was given over to MX, and the Bending Magnet beamline BM14 [3]. The latter was (and still is, see below) a variable energy facility dedicated to the phasing of

* Contribution to the Focus Point on "Status of third-generation synchrotron crystallography beamlines: An overview" edited by Gaston Garcia.

[a] e-mail: leonard@esrf.fr

[1] http://www.esrf.eu/.

[2] See http://www.esrf.eu/Accelerators/Operation/Modes for details.

macromolecular crystal structures using Anomalous Dispersion techniques (MAD/SAD). The small, highly collimated X-ray beam provided by ID02 and ID13 enabled the study of smaller crystals and crystals with larger unit cells than had previously been the case (*e.g.* bacteriorhodopsin [4], nucleosome core particle [5]). The construction of BM14, coupled with the availability of CCD detectors, developments in the cryo-cooling of crystals [6] and advances in the development of structure solution exploiting anomalous scattering [7,8], helped establish MAD/SAD as the pre-eminent techniques for the *de novo* elucidation of the crystal structures of biological macromolecules.

The success of ID02 and BM14 provided the impetus for the construction, in 1998, of four undulator-based beamlines dedicated to MX at ID14 [9]. The "Quadriga" complex, based around three undulators, mounted in series, as X-ray sources and diamond beam-splitting monochromators, provided three fixed-energy beamlines (ID14-1, ID14-2, ID14-3) and one tuneable facility, ID14-4, with a limited ($\sim$ 9–$\sim$15 keV) energy range. While, to date, ID14 has probably been the most successful beamline complex ever built for MX[3], the inherent interdependence of the four end stations —changing energy, and thus the undulator gap on ID14-4, affected the intensity at the sample position of the other three beamlines— the limited energy range of ID14-4, and the rather large beam sizes at the sample position were somewhat disadvantageous. Addressing these areas led directly to the construction and commissioning of the fully tuneable MAD beamline ID29 [10] in 2001 and, later, to the commissioning of two independent beamlines (ID23-1 and ID23-2) constructed around a canted undulator set-up. ID23-1 [11], like ID29, is a fully independent and tuneable MAD beamline. ID23-2 [12] was the world's first micro-focus beamline fully dedicated to MX and built as a direct result of the pioneering work carried out on the ESRF beamline ID13 [13].

In 2008, the ESRF launched Phase I of its Upgrade Program[4], an integral part of which was the replacement of the ageing ID14 "Quadriga" complex with a new suite of three beamlines on the straight-section ID30 [14]. Of the four end stations being constructed, ID30A-1 (see below) entered operation in July 2014, ID30A-3 became operational in December 2014 and ID30B is due to begin operation in the Spring of 2015.

Facilities for structural biology at the ESRF are not limited to experimental resources for MX. Phase I of the ESRF upgrade program has also seen the construction of BM29 [15] a beamline for increasingly popular experiments on solutions of biological macromolecules that exploit Small Angle X-ray Scattering (BioSAXS). BM29 offers rapid access to automated high-throughput SAXS data collection and is equipped with robotic sample handling [16] that also enables on-line size exclusion chromatography [17]. On BM29 data collection, analysis and initial processing is facilitated for all users with the results of automated pipelines presented in the BioSAXS Laboratory Information Management System (LIMS) ISPyBB [18]. The ESRF also operates, in collaboration with the Institut de Biologie Structurale (IBS, Grenoble), ID29S —also known as the Cryobench— a facility for on- or off-line investigations of solutions and/or crystals of macromolecules using a variety of spectroscopic techniques [19]. As both BM29 and the ID29S Cryobench have already been extensively described they will not be illustrated any further here.

All of the ESRF's facilities for structural biology, including BM29 and ID29S, can be accessed either on a public or proprietary basis. Applications for public access beam time are via the ESRF's Beam-time Allocation Panel (BTAP) mechanism. Here, the Block Allocation Group (BAG) mechanism[5], pioneered at ESRF, allows larger laboratories or groupings of laboratories to be pre-allocated significant amounts of beam time based on the peer review (every year) of previous use of the ESRF. For smaller laboratories, the ESRF's Rolling Access Mechanism[5] allows applications for beam time to be submitted at *any* time. Peer review of Rolling Access applications by the BTAP generally takes place within two weeks of receiving an application and, if beam time is awarded, this is usually scheduled within 8 weeks. Provided that a BAG or Rolling Access proposal is from a laboratory in a Member Country or Scientific Associate of the ESRF, expenses related to participation in an experimental session (travel to/from Grenoble, accommodation costs, meals) are reimbursed by ESRF up to agreed levels[6].

Proprietary access [20] to the ESRF's facilities for structural biology is via the ESRF's Business development office (BDO). Industrial clients of the ESRF's MX beamlines —mainly from the pharmaceutical industry— can either purchase beam time directly, carrying out experiments themselves, or they can take advantage of the MXpress data collection service. Here, samples are shipped to the ESRF, data collections are carried out by ESRF staff and the resulting raw diffraction images and reduced data are downloaded by clients directly to their home laboratory.

2 Beamlines dedicated to macromolecular crystallography

2.1 Overview

The ESRF's facilities for MX and BioSAXS (fig. 1) are operated by staff of the Joint Structural Biology Group (JSBG), a collaboration between the ESRF and EMBL Grenoble Outstation. By mid-2015, six ESRF end stations fully

[3] Diffraction data collected on ID14 has been responsible for more than 5000 depositions in the Protein Data Bank (PDB, `http://www.rcsb.org/pdb/home/home.do`) contributing to more than 3500 publications in peer-reviewed journals.

[4] `http://www.esrf.eu/about/upgrade/documentation/purple-book`.

[5] For details of BAG and Rolling Access mechanisms for application for beam time at ESRF see (`http://www.esrf.eu/UsersAndScience/UserGuide/Applying/MXApplications`).

[6] `http://www.esrf.eu/UsersAndScience/UserGuide/FinancialAssistance`.

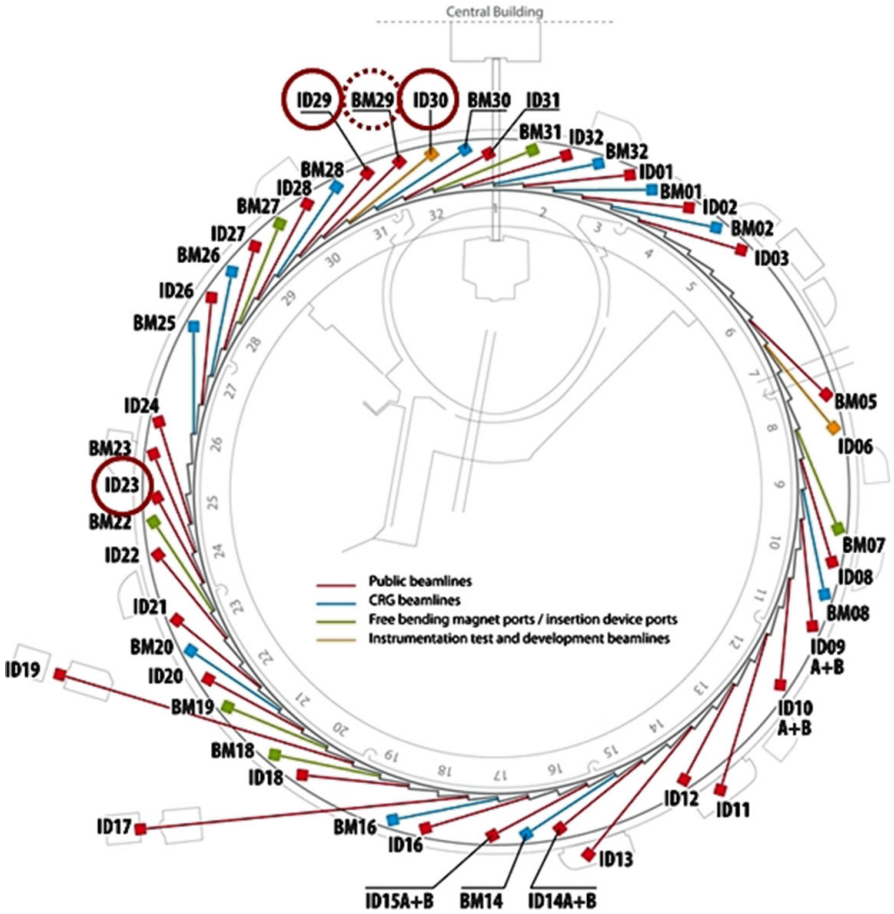

Fig. 1. A representation of the ESRF storage ring highlighting the location of its facilities for macromolecular crystallography (solid circles). Also highlighted (dashed circle) is the location of the BioSAXS beamline BM29. The ID29S cryobench is co-located with ID29. Figure courtesy of the ESRF Communication Unit.

dedicated to MX will be open for public or proprietary access (see table 1 for general characteristics). Additionally, beam time for MX experiments is available on two Collaborative Research Group (CRG) beamlines BM14[7] and BM30A[8] which use bending magnet sources of X-rays.

As can be seen from table 1, when fully operational the ESRF's MX facilities will provide a broad range of options for structural biologists with high flux end stations offering a variety of beam sizes —including micro-focus— at the sample position and access to techniques such as screening and data collection from crystals *in situ* (*i.e.* in crystallisation plates), on-line UV-visible absorption and Raman spectroscopies, and automatic, multi-sample data collection, processing and analysis. Figure 2 illustrates how the ESRF's MX facilities are typically used for diffraction data collection and resulting structure solution from samples meeting the requirements of biosafety levels 1 and 2 only. As can be seen (fig. 2(A)), even on the fully tuneable ID29 and ID23-1 end stations the great majority of experiments are aimed at the collection of data for structure solution using the Molecular Replacement technique. Indeed, the explicit —as annotated in depositions in the Protein Data Bank [21]— use of anomalous scattering accounts for only around 10% of crystal structure determinations based on diffraction data collected on either ID23-1 or ID29. Figure 2(B) illustrates how the wavelength/energy tuneability is generally exploited. Over 75% of all data collection is carried out in the wavelength range 0.95–1.0 Å (*i.e.* close to, but not necessarily targeting, the Se-K absorption edge). Experiments carried out beyond this wavelength range target the collection of diffraction data around a wide range of absorption edges. However, peaks in the distribution shown in fig. 2(B) indicate, as might be expected, that the most common of these are Br-K ($\lambda \sim 0.92$ Å), Pt-L_{III} ($\lambda \sim 1.07$ Å), Zn-K ($\lambda \sim 1.28$ Å) and Fe-K ($\lambda = 1.74$ Å). A significant number of experiments are carried at $\lambda > 1.8$ Å. These probably aim at exploiting the small anomalous signal available from sulphur and phosphorous atoms at such wavelengths (S-SAD, [22]) for structure solution. Experiments at very

[7] http://www.embl.fr/services/synchrotron_access/bm14/.
[8] http://www.esrf.eu/UsersAndScience/Experiments/CRG/BM30A.

Table 1. A summary of the characteristics of the ESRF's current facilities for macromolecular crystallography. For ID23-1 and ID29 beam sizes in parentheses are achievable using apertures. Flux at sample position is as measured for the largest beam size available at a storage ring current of ~ 200 mA. For the end stations ID23-1 and ID29 flux measurements were carried out at the Pt L_{III} absorption edge (11.563 keV).

Beamline	Energy range [keV]	Beam size (FWHM) at sample position (μm; H × V)	Flux at sample position (ph/s)	Detector	Frame rate (Hz)	Comments
ID23-1[(a)]	6–20	50 × 40 (30; 20; 10)	3×10^{12}	Pilatus 6M	25	MAD/SAD
ID23-2[(b)]	14.2	5.3 × 9.6	1×10^{12}	Pilatus3 2M	250	μ-beam
ID29[(a)]	6–20	60 × 30 (30; 20; 10)	1×10^{13}	Pilatus 6M	25	MAD/SAD
MASSIF-1[(c)]	12.8	15–150	5×10^{12}	Pilatus3 2M	250	HTP automatic data collection
MASSIF-3[(c)]	12.9	15	2×10^{13}	Eiger 4M	750	HTP automatic data collection; serial synchrotron crystallography
ID30B[(d)]	6–20	20–200	$\sim 10^{13}$	Pilatus3 6M	100	MAD/SAD variable beam size

(a) Beam size measured at the sample position by scanning a 5 μm pin-hole vertically and horizontally through the X-ray beam.
(b) Beam size measured at the sample position by scanning a 200 μm diameter tungsten wire (ID23-2) vertically and horizontally through the X-ray beam.
(c) Beam size (maximum shown) measured using YAG (Yttrium Aluminium Garnet) scintillator screen inserted at sample position.
(d) Estimated from ray-tracing.

short wavelength ($\lambda \sim 0.6$–0.7 Å) are probably designed for the collection of ultra-high-resolution diffraction data from crystals of biological macromolecules.

All ESRF-owned end stations dedicated to MX are furnished with fast-readout pixel array detectors (DECTRIS, Switzerland) and are highly automated. Currently all end stations, with the exception of MASSIF-1, are equipped with micro- or mini-diffractometers (MD2, MD2S, MD2M; Arinax, Moirans, France[9], sphere of confusion (SOC) less than 2 μm) in combination with sample mounting robots. Sample mounting on ID23-1, ID23-2, ID29 and MASSIF-3 is currently achieved using EMBL-ESRF SC3 robots [23] each with a capacity of 50 SPINE standard sample holders. Upon entering user operation in 2015, sample changing on ID30B will be effected with an EMBL-developed robotic sample changer coupled to an ESRF-developed High Capacity Dewar (HCD) capable of holding up to 240 SPINE standard sample holders. On MASSIF-1 an ESRF-developed robot, the RoboDiff, to be fully described elsewhere, acts as both sample changer and diffractometer (designed with a SOC of the data collection rotation axis comparable to those of the MD2, MD2S and MD2M goniometers installed elsewhere, see above) and is operated in conjunction with an HCD.

The sample environment (fig. 3) at all end stations also includes a Cryostream 700 series cryocooler (temperature range 80–400 K; Oxford Cryosystems, Oxford, UK) with annealing blade [24] mounted and on-axis viewing set-ups. Fluorescence detectors used either for scanning of absorption edges for MAD/SAD experiments (tuneable energy end stations) or for the measurement and subsequent automatic analysis of X-ray fluorescence spectra [25] will be installed on all end stations.

Experiment control and tracking on all end stations is achieved via a combination of the MXCuBE graphical user interface [26] —recently upgraded to MXCuBE2 [27]— and the ISPyB database [28]. As already described for MXCuBE [26], MXCuBE2 links beamline control hardware to graphical representations with low-level control achieved via connection to TACO or TANGO[10] servers and to the macro-language SPEC[11] and allows for the user-friendly control of all beamline components, regardless of any difference in the nature of these on the different end stations. For example, the realignment of X-ray beam and goniometer rotation axis is a "single-click" procedure while changing energy on tuneable energy end stations is a completely automatic procedure requiring only input by the user of the photon energy desired or the setting up in the MXCuBE2 "queue" (see below) of a multi-wavelength experiment.

[9] See `http://www.arinax.com/en/scientific-instrumentation/product-portfolio.html#MD2M_product_description` for details.
[10] `http://www.tango-controls.org/`.
[11] `http://www.certif.com/`.

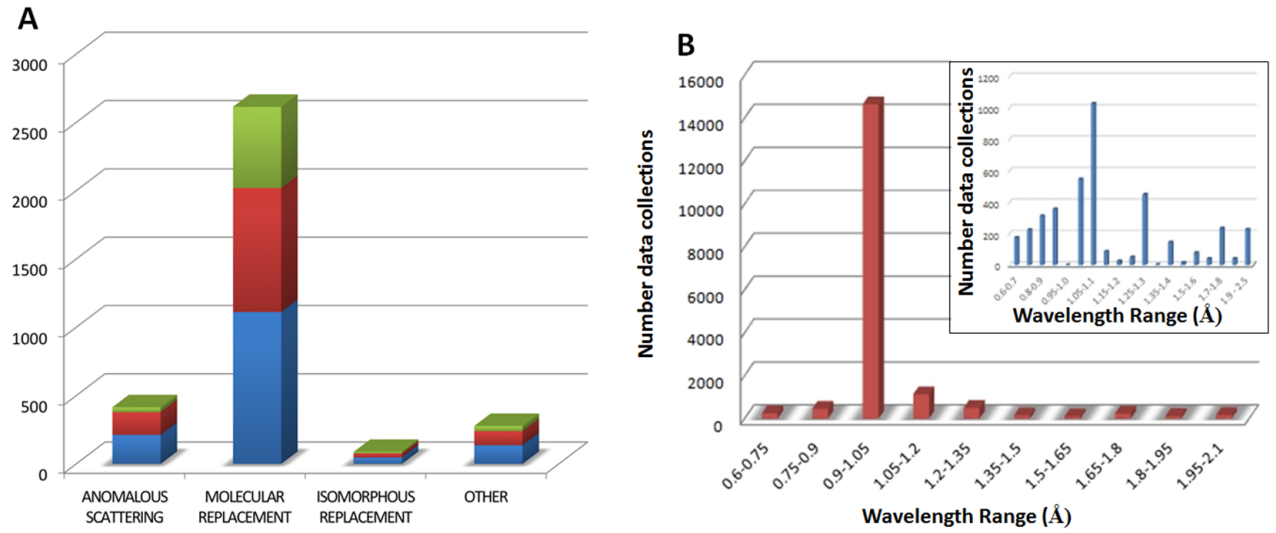

Fig. 2. (A): Even on the fully tuneable ID29 (blue) and ID23-1 (red) end stations the great majority of experiments result in structure determination using MR. Conversely, on the fixed wavelength ID23-2 (green) a non-negligible number of experiments result in structure solution based on the use of anomalous scattering. (B): Over 75% of all data collection on ID29 is performed at wavelengths close to that of the Se-K absorption edge. As shown in the inset (in which the number of collections close to Se-K edge has been truncated to 1000) experiments carried out outside this wavelength range most commonly target the absorption edges: Br-K ($\lambda \sim 0.92$ Å), Pt-LIII ($\lambda \sim 1.07$ Å), Zn-K ($\lambda \sim 1.28$ Å), Fe-K ($\lambda = 1.74$ Å). A significant number of S-SAD experiments are carried at $\lambda > 1.8$ Å. Experiments at very short wavelength ($\lambda \sim 0.6$–0.7 Å) are mainly aimed at the collection of ultra-high-resolution diffraction data from crystals of biological macromolecules.

The centring of crystals in the X-ray beam is performed using either a simple (for users!) 3-click approach following a round of automatic centring carried out upon sample mounting or, in more problematical cases (*i.e.* very small crystals, lens effects) or when desired by users, via a cartography-based approach [29] implemented in a workflow (see below).

In MXCuBE2 the preparation and execution of experiments is performed using a "Queuing" function. Different steps in a particular experiment are added to a queue either explicitly by the user or, as is more often the case, as the result of a previous step (*i.e.* successful determination of a data collection strategy [30] will add data collection using the strategy determined as the next step in the queue). The different steps can then be daisy-chained together and performed automatically with no user intervention or, if the user prefers, each step is performed only when he/she has checked that the outcome of a previous step is what is desired.

More complicated procedures including cartography-based crystal centring [29], line and mesh scans, helical data collections [10,12] dehydration protocols [31] and crystal alignment using mini-kappa goniometers [32] are carried out via a series of pre-installed workflows [33] available in MXCuBE2 on all MX beamlines (fig. 4). The workflows themselves are best seen as a collection of beamline "Wizards" which guide users through the preparation and execution of more complex experiments while, at the same time, allowing them a relatively free hand in terms of setting parameters relevant to an experiment. Experiments exploiting the dehydration workflows (see [34] for details) require both installation of a HC1c humidity controller (Arinax, Moirans, France) [35] and the allocation of sufficient beam time. Thus, while dehydration trials can be carried out autonomously by users, prior notice of the intention to carry out such an experiment is required.

The MXCuBE2/ISPyB combination also enables remote control of all end stations [26], the provision of services for proprietary research [20] and the fully automatic, "hands-off" data collection service recently implemented on MASSIF-1. In this latter service, samples are shipped to the ESRF and, for each sample, information regarding the experiment required uploaded into ISPyB by the external user. On the day of the experiment the samples are loaded by beamline staff into the HCD installed on MASSIF-1 and the information contained in ISPyB concerning these downloaded to the MxCuBE2 GUI. All actions required for any given crystal are then carried out automatically[12]. As is implied by the term "hands-off", users do not control the beamline during experimental sessions on MASSIF-1. For experiments, including those exploiting remote access, on all other ESRF MX end stations a specifically assigned Local Contact, available between 08h00 and 22h00, is responsible for the preparation and testing of the end station, the provision —if necessary— of advice on carrying out experiments and the resolution of problems due to malfunctioning beamline hardware or software.

[12] see `http://www.esrf.fr/MXPressE` for further details and timings.

Fig. 3. The sample environment of ID29 (top) comprises a micro-diffractometer with mini-kappa goniometer mounted, a SC3 sample mounting robot, a fast-readout pixel array detector, a Cryostream 700 series cryocooler with annealing blade and a fluorescence detector. The sample environments of ID23-1 (middle) and ID23-2 (bottom) comprise the same elements based around a mini-diffractometer.

Unless an end-station user chooses otherwise, all diffraction data collected at the ESRF MX beamlines are automatically processed and analysed on parallel computer clusters using the GrenADes [36] and EDNA (unpublished) autoprocessing packages providing a rapid feedback on experiments performed. Furthermore, if anomalous signal is detected, automatic SAD phasing is also attempted [36]. Results of data processing are subsequently displayed in ISPyB from which files containing scaled intensity and/or structure factor data —along with relevant log files— are made available for download to be used in downstream processes.

Workstations in the control cabins on all end stations except MASSIF-1 offer access to software for the manual (re-)processing of diffraction images (XDS [37], iMOSFLM [38]) and for structure solution and refinement (CCP4 [39], PHENIX [40], SHELX [41]). Workstations dedicated for the backup of data are also available[13]. Raw and processed data are stored on the ESRF's Networked Interactive Computing Environment (NICE) for 30 days after an experiment.

[13] `http://www.esrf.fr/home/UsersAndScience/Experiments/MX/How_to_use_our_beamlines/Prepare_Your_Experiment/Backup/esrf-backup-software.html`.

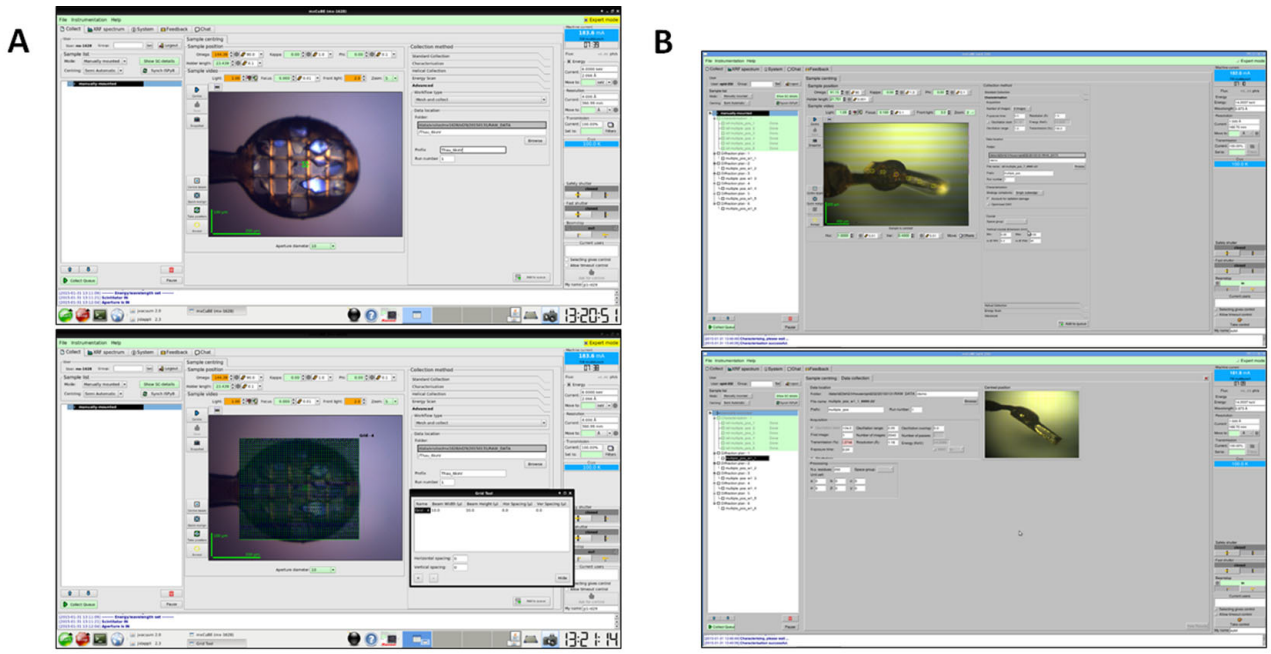

Fig. 4. In addition to the procedures described in the main text, MXCuBE2 also provides workflows for multi-crystal (A) or multi-position (B) data collection. In the former a mesh scan is used to automatically determine the positions of many crystals contained in the same loop. In the latter, 3-click centring is used to define different positions for data collection on the same crystal. In (B), the MXCuBE2 queuing function (white rectangle, left-hand side) is first used to set up the characterisation of the diffraction quality (results for one position shown in the bottom panel) at each position. The strategies determined are added to the queue with the resulting series of data collections carried out automatically if desired.

During this time, if necessary, computers on the NICE infrastructure can be accessed through either SSH (Secure Shell) or NX protocols for further data processing and analysis or data transfer to the home laboratory using File Transfer Protocol (FTP) or Secure Copy (SCP). After this 30 day period all data are transferred to tape storage from which they can be retrieved, upon request, during a maximum period of 6 months.

In addition to facilities for MX, BioSAXS (BM29) and *in cristallo* spectroscopy (Cryobench), ancillary laboratory space for simple sample preparation and manipulation is available in the ESRF Experimental Hall as well as at the EMBL Grenoble Outstation. Access to the latter is requested via the "A-Form" completed by external users before all experimental sessions at ESRF. We have also recently commissioned a service for the high-pressure cryocooling of crystals [42] which is now also available to external users of the ESRF's MX facilities.

2.2 Future plans

Once constructed and commissioned the ESRF's MX beamlines are in an almost continuous state of improvement and refurbishment. In particular detectors are upgraded to the latest version available as soon as funding allows. The MXCuBE2 beamline control software and ISPyB database are continuously evolving. Moreover, the recent transfer of motor control on ID23 and ID29 from DPAP to ICEPAP modules has enabled faster mesh and helical scanning that allows users to take full advantage of the fast-readout detectors (see above) installed on all end stations.

Beamlines are also occasionally removed from operation in order to upgrade optical elements so that users of the ESRF's MX beamlines continue to benefit from well-defined and stable X-ray beam characteristics. Examples of this are the refurbishment of the ID14-4 optics hutch [43] (this beamline has since closed), the recent replacement of both mirrors in the Kirkpatrick-Baez focusing element of ID23-2 which resulted in a 4-fold increase in flux at the sample position and, planned for 2016, the provision of a high flux, sub-micron size X-ray beam on the same end station.

Longer term plans for the ESRF's MX end stations clearly revolve around the planned Phase II Upgrade of the ESRF[14] which will reduce the horizontal emittance of the electron beam in the storage ring by a factor of ~ 30. The commensurate reduction in X-ray beam size and X-ray beam divergence —particularly on low beta straight sections (*i.e.* ID23, ID29)— will allow the construction of a new generation of ESRF MX beamlines with flux densities at the sample position ~ 5 orders of magnitude higher than is currently the case (table 2). Such beamlines will be optimised

[14] `http://www.esrf.eu/home/about/upgrade/documentation/orange-book.html`.

Table 2. The potential beam characteristics of ID29 after the proposed Phase-II upgrade of the ESRF storage ring, compared with its current status.

	Current status	New lattice (current optics)	New lattice (perfect optics)	New lattice (50:1)
Source size (FWHM; H × V; μm^2)	115 × 13.2	59 × 11	59 × 11	59 × 11
Divergence (r.m.s. H × V; μrad^2)	104 × 6.1	7.4 × 5.3	7.4 × 5.3	7.4 × 5.3
Demagnification ratio	3:1	3:1	3:1	50:1
Beam size @ sample (μm^2)	60 × 30	30 × 25	20 × 4	1.2 × 0.2
Flux @ sample (ph/s)	$\sim 1 \times 10^{13}$	$\sim 1 \times 10^{14}$	$\sim 1 \times 10^{14}$	$\sim 1 \times 10^{14}$
Flux density @ sample (ph/s/μm^2)	7.0×10^9	1.7×10^{11}	2.1×10^{12}	2.4×10^{14}
Absorbed dose rate (Gy/s)	3.2×10^6	7.7×10^7	9.6×10^8	1.2×10^{11}
Time to reach Henderson limit (s)	6.3	0.26	0.021	0.0002

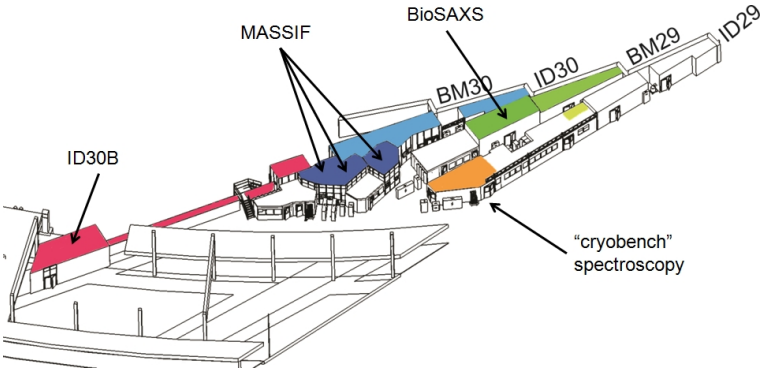

Fig. 5. The "MX Village" centred around ESRF straight sections 29 and 30 comprises ID29, ID29S, BM29 (BioSAXS), the MASSIF complex (ID30A) and the MAD beamline ID30B. The French beamline for Investigation of Proteins (FiP) sited on BM30 (see main text) is also close to the MX Village.

for techniques such as synchrotron serial crystallography (SSX), probably best described as the collection and merging of partial data sets as small as a single image from many (hundreds to tens of thousands) microcrystals to produce a complete data set [44,45]. The availability of such beamlines, when coupled with continuous readout X-ray detectors, may also lead to a resurgence in time-resolved studies employing pump-probe methods.

3 ID30

As mentioned above, the end stations on ID30 are the newest facilities for MX in the ESRF's portfolio of beamlines. Constructed on a canted-undulator straight section ID30 combines knowledge gained from the operation of ID14 and ID23 to provide two independent X-ray sources. The first serves two ID30A fixed-energy end stations (MASSIF-1, MASSIF-3), the second delivers photons for ID30B —a tuneable energy end station (table 1, fig. 5, [14]).

The MASSIF beamlines were originally designed as facilities for sample evaluation and the screening of the diffraction quality of samples prior to the distribution of the best ones to ID23, ID29 or ID30B for full data collection. The advent of fast-readout pixel detectors [46] and extremely fast so-called "shutterless" data collection [47] has morphed MASSIF-1, extremely successfully, into a resource that provides both a sample screening facility and a fully automatic, hands-off data collection service (see sect. 2.1 above). MASSIF-3, while offering a service for the automatic screening of microcrystals (3–10 μm in size), will also be operated as a traditional beamline, the characteristics of which complement and reinforce the capabilities of our other micro-focus facility, ID23-2. Additionally, the small beam size ($\sim 15\,\mu$m diameter) and high flux ($> 10^{13}$ ph/s) characteristics of MASSIF-3 coupled with the installation of an Eiger 4M detector (Dectris, Switzerland) with a maximum frame-rate of 750 Hz will make MASSIF-3 an ideal vehicle for initial experiments exploiting SSX.

The tuneable energy beamline ID30B —the replacement for the highly successful ID14-4, which is now closed— will provide both a high photon flux ($\sim 10^{13}$ ph/s) and variable spot size (20 to 200 μm^2) at the sample position. As well as "standard" experiments in MX, ID30B will also (from mid-2015) provide access to *in situ* screening and data collection. Although this functionality of ID30B is still in the development phase, current plans are that control of

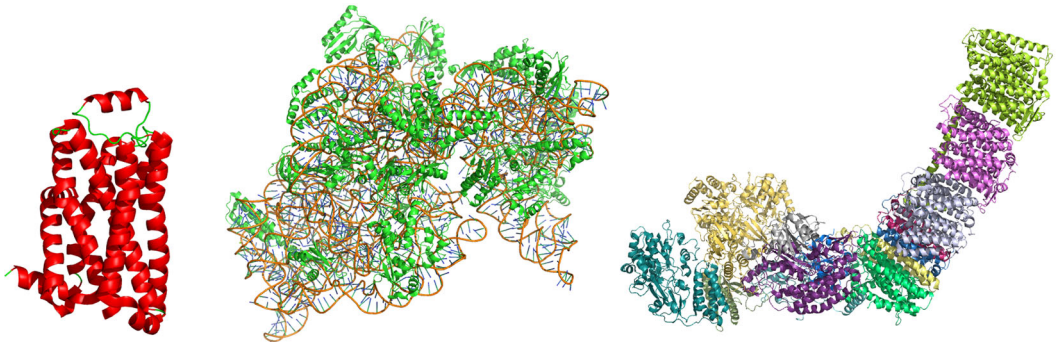

Fig. 6. Highlights from 15 years of experiments at the ESRF's facilities for MX include the elucidation of the crystal structures of, from left to right: GPCRs (β1-adrenergic receptor [57], PDB entry 2RH1, data collected on ESRF ID23-2), the 30S ribosomal subunit in complex with antibiotics (PDB entry 1FJG [64], data collected on ESRF ID14-4) and the entire respiratory Complex 1 (PDB entry 4HEA [58], data collected on ESRF ID29).

both *in situ* diffraction testing and data collection are integrated into MXCuBE2 and that *in situ* diffraction testing and data collection will be possible from several types of crystallisation plate.

Although situated on a high beta straight section, the planned Phase II upgrade of the ESRF will also be beneficial to the MASSIF end stations and to ID30B. Vertical focusing for all three MASSIF end stations is currently achieved using a set of white beam compound refractive lenses (CRLs). For MASSIF-1 horizontal focusing is achieved using CRLs which currently accept only $\sim 50\%$ of the beam. The reduced source size of a Phase II-upgraded ESRF would allow the entire beam to be accepted. This and the commensurately reduced beam size at the sample position will result in an increase in flux density for MASSIF-1 by a factor of ~ 2.5. On MASSIF-3 horizontal focusing is carried out using a multi-layer mirror. Here, a Phase-II ESRF will allow both horizontal and vertical focusing to be achieved using CRLs. This will lead to an increase in flux at the MASSIF-3 sample position.

On ID30B focusing in the vertical direction is achieved using CRLs in a transfocator set-up downstream of a channel-cut Si(111) monochromator ~ 60 m from the source. Focusing in the horizontal direction is carried out using an elliptical mirror 97.5 m from the source and 2.5 m from the sample position. This set-up was chosen because the acceptance of horizontally focusing CRLs with the present machine lattice is unfavourable. On a Phase II-upgraded ESRF storage ring vertical and horizontal focussing could be achieved by two sets of CRLs —both accepting the entire beam— mounted in a vessel ~ 60 m from the source. Beam divergence at the sample position would thus be much reduced facilitating the collection of diffraction data to very low resolution using very long crystal to detector distances.

4 Examples of science carried out at the ESRF MX beamlines

Science carried out at the ESRF's MX beamlines falls into two categories: that done by ESRF staff and that done by external visitors to our facilities. While many ESRF staff carry out traditional structural biology projects supported by access to synchrotron beamlines and the platforms of the Partnership for structural biology[15], much of their scientific effort is devoted to the development of methodology for diffraction data collection [30,48–50] and structure solution [22, 51–53] as well as to improvements to beamline software tools (see sect. 2.1), ensuring that external users have the optimal experimental set-ups for their visits to our facilities.

To date, diffraction data collected at ESRF MX beamlines has been responsible for more than 10000 depositions in the Protein Data Bank[16]. Particular highlights over the last decade or so are undoubtedly represented by the work on the determination of crystal structures of the ribosome [54,55] that led to the award of a share in the Nobel Prize for chemistry in 2009 for Prof. Ada Yonath and Prof. Venki Ramaksrishnan and work on the determination of the crystal structures of G-coupled Protein Receptors (GPCRs, [56,57]) some of which led to a share in the Nobel Prize for chemistry in 2012 for Brian Kobilka. However, science carried out by the ESRF's external user community covers the whole gamut of structural biology, resulting in structural information on large numbers of biologically important systems (fig. 6). These include very large integral membrane proteins [58,59], protein complexes of high medical relevance [60], and proteins that may be of interest in the development of biocatalysts for renewable energy generation [61]. The high flux densities available on the ESRF's MX beamlines have also facilitated the study of the crystal structures of biological macromolecules at sub-atomic resolution [62,63].

[15] `http://www.psb-grenoble.eu/`.

[16] See `http://biosync.sbkb.org/stats.do?stats_sec=RGNL&stats_focus_lvl=SITE&stats_site=ESRF` for details.

5 Conclusions

The ESRF's facilities for MX operated by the ESRF/EMBL Joint Structural Biology Group have provided a major contribution to European Structural Biology since the mid-1990s. Currently these facilities comprise six end stations grouped around three straight sections (ID23, ID29, and ID30) and provide experimental resources for an extremely wide range of applications. These encompass everything from the screening of the diffraction qualities of newly obtained crystals through standard diffraction data collection from robust well-characterised systems to data collection and structure solution from microcrystals. Moreover, combining recent developments in hardware and software has resulted, in an automatic diffraction data collection service allowing users to screen and collect diffraction data from hundreds of crystals without physical intervention, thus allowing more efficient use of beam time. These developments coupled with the planned Phase-II Upgrade of the ESRF storage ring will also open the doors to new types of experiments such as synchrotron serial crystallography, multi-crystal data collections and much more.

The status of the ESRF's facilities for MX described above would not have been possible without the extremely hard work of the technical staff of the ESRF Structural Biology Group (Hugo Caserotto, Fabien Dobias, Thierry Giraud, Mario Lentini, John Surr), the technical staff of the EMBL Grenoble Outstation Synchrotron Instrumentation Group, the ESRF Beamline Control Unit (Matias Guijarro, Antonia Beteva, Marcus Oskarsson), the ESRF Data Analysis Unit (Olof Svensson), the staff of the ESRF ISDD, particularly Pascal Theveneau, Trevor Mairs and Carole Clavel and the staff of the ESRF MX-BDO (Stéphanie Monaco-Malbet, Emilie Poudevigne). The authors gratefully acknowledge the contributions of all those named above. The purchase of the PILATUS3 6M detector for ID30B was partly supported by the French Infrastructure for Integrated Structural Biology Initiative FRISBI (ANR-10-INSB-05-02).

References

1. J. Lescar *et al.*, ESRF Newsletter **28**, 12 (1997).
2. H. Belrhali *et al.*, ESRF Newsletter **28**, 15 (1997).
3. V. Biou *et al.*, ESRF Newsletter **28**, 21 (1997).
4. E. Pebay-Peyroula *et al.*, Science **277**, 1676 (1997).
5. K. Luger *et al.*, Nature **389**, 251 (1997).
6. H. Hope, Acta Crystallogr. B-Struct. Sci. **44**, 22 (1988) doi:10.1107/S0108768187008632.
7. W.A. Hendrickson, C.M. Ogata, Macromol. Crystallogr. A **276**, 494 (1997) doi:10.1016/S0076-6879(97)76074-9.
8. J.L. Smith, Curr. Opin. Struct. Biol. **1**, 1002 (1991) doi:10.1016/0959-440X(91)90098-E.
9. S. Wakatsuki *et al.*, J. Synchrotron Radiat. **5**, 215 (1998) doi:10.1107/S0909049597018785.
10. D. de Sanctis *et al.*, J. Synchrotron Radiat. **19**, 455 (2012) doi:10.1107/S0909049512009715.
11. D. Nurizzo *et al.*, J. Synchrotron Radiat. **13**, 227 (2006) doi:10.1107/S0909049506004341.
12. D. Flot *et al.*, J. Synchrotron Radiat. **17**, 107 (2010) doi:10.1107/S0909049509041168.
13. A. Perrakis *et al.*, Acta Crystallogr. Sect. D-Biol. Crystallogr. **55**, 1765 (1999) doi:10.1107/S0907444999009348.
14. P. Theveneau *et al.*, J. Phys.: Conf. Ser. **425**, (2013) doi:10.1088/1742-6596/425/1/012001.
15. P. Pernot *et al.*, J. Synchrotron Radiat. **20**, 660 (2013) doi:10.1107/S0909049513010431.
16. A. Round *et al.*, Acta Crystallogr. D-Biol. Crystallogr. **71**, 67 (2015) doi:10.1107/S1399004714026959.
17. A. Round *et al.*, Acta Crystallogr. D-Biol. Crystallogr. **69**, 2072 (2013) doi:10.1107/S0907444913019276.
18. A. De Maria Antolinos *et al.*, Acta Crystallogr. D-Biol. Crystallogr. **71**, 76 (2015) doi:10.1107/S1399004714019609.
19. D. von Stetten *et al.*, Acta Crystallogr. D-Biol. Crystallogr. **71**, 15 (2015) doi:10.1107/S139900471401517X.
20. S. Malbet-Monaco *et al.*, Acta Crystallogr. D-Biol. Crystallogr. **69**, 1289 (2013) doi:10.1107/S0907444913001108.
21. H.M. Berman *et al.*, Nucl. Acids Res. **28**, 235 (2000) doi:10.1093/Nar/28.1.235.
22. E. Micossi, W.N. Hunter, G.A. Leonard, Acta Crystallogr. D-Biol. Crystallogr. **58**, 21 (2002) doi:10.1107/S0907444901016808.
23. F. Cipriani *et al.*, Acta Crystallogr. D-Biol. Crystallogr. **62**, 1251 (2006) doi:10.1107/S0907444906030587.
24. T. Giraud *et al.*, J. Appl. Crystallogr. **42**, 125 (2009) doi:10.1107/S0021889808040958.
25. G.A. Leonard *et al.*, J. Appl. Crystallogr. **42**, 333 (2009) doi:10.1107/S0021889809001721.
26. J. Gabadinho *et al.*, J. Synchrotron Radiat. **17**, 700 (2010) doi:10.1107/S0909049510020005.
27. D. de Sanctis, G. Leonard, in *Notiziario Neutroni e Luce di Sincrotrone* Vol. **19** (Consiglio Nazionale delle Ricerche, 2014) p. 24.
28. S. Delageniere *et al.*, Bioinformatics **27**, 3186 (2011) doi:10.1093/bioinformatics/btr535.
29. M.W. Bowler *et al.*, Acta Crystallogr. D-Biol. Crystallogr. **66**, 855 (2010) doi:10.1107/S0907444910019591.
30. G.P. Bourenkov, A.N. Popov, Acta Crystallogr. D-Biol. Crystallogr. **66**, 409 (2010) doi:10.1107/S0907444909054961.
31. J. Sanchez-Weatherby *et al.*, Acta Crystallogr. D-Biol. Crystallogr. **65**, 1237 (2009) doi:10.1107/S0907444909037822.
32. S. Brockhauser *et al.*, Acta Crystallogr. D-Biol. Crystallogr. **69**, 1241 (2013) doi:10.1107/S0907444913003880.
33. S. Brockhauser *et al.*, Acta Crystallogr. D-Biol. Crystallogr. **68**, 975 (2012) doi:10.1107/S090744491201863x.
34. M.W. Bowler *et al.*, Cryst. Growth Des. **15**, 1043 (2015) doi:10.1021/cg500890r.
35. S. Russi *et al.*, J. Struct. Biol. **175**, 236 (2011) doi:10.1016/j.jsb.2011.03.002.

36. S. Monaco *et al.*, J. Appl. Crystallogr. **46**, 804 (2013) doi:10.1107/S0021889813006195.
37. W. Kabsch, Acta Crystallogr. D-Biol. Crystallogr. **66**, 125 (2010) doi:10.1107/S0907444909047337.
38. T.G. Battye *et al.*, Acta Crystallogr. D-Biol. Crystallogr. **67**, 271 (2011) doi:10.1107/S0907444910048675.
39. M.D. Winn *et al.*, Acta Crystallogr. D-Biol. Crystallogr. **67**, 235 (2011) doi:10.1107/S0907444910045749.
40. P.D. Adams *et al.*, Acta Crystallogr. D-Biol. Crystallogr. **66**, 213 (2010) doi:10.1107/S0907444909052925.
41. G.M. Sheldrick, Acta Crystallogr. A **64**, 112 (2008) doi:10.1107/S0108767307043930.
42. P. van der Linden *et al.*, J. Appl. Crystallogr. **47**, 584 (2014) doi:10.1107/S1600576714000855.
43. A.A. McCarthy *et al.*, J. Synchrotron Radiat. **16**, 803 (2009) doi:10.1107/S0909049509035377.
44. C. Gati *et al.*, IUCrJ **1**, 87 (2014) doi:10.1107/S2052252513033939.
45. F. Stellato *et al.*, IUCrJ **1**, 204 (2014) doi:10.1107/S2052252514010070.
46. C. Broennimann *et al.*, J. Synchrotron Radiat. **13**, 120 (2006) doi:10.1107/S0909049505038665.
47. G. Hulsen *et al.*, J. Appl. Crystallogr. **39**, 550 (2006) doi:10.1107/S0021889806016591.
48. R. Giordano *et al.*, Acta Crystallogr. D-Biol. Crystallogr. **68**, 649 (2012) doi:10.1107/S0907444912006841.
49. J.L. Ferrer *et al.*, Expert Opin. Drug Discov. **8**, 835 (2013) doi:10.1517/17460441.2013.793666.
50. M.G. Bowler, M.W. Bowler, Acta Crystallogr. F **70**, 127 (2014) doi:10.1107/S2053230X13032007.
51. G.A. Leonard *et al.*, Acta Crystallogr. D-Biol. Crystallogr. **61**, 388 (2005) doi:10.1107/S0907444905000429.
52. R.B.G. Ravelli *et al.*, J. Synchrotron Radiat. **12**, 276 (2005) doi:10.1107/S0909049505003286.
53. D. de Sanctis, M.H. Nanao, Acta Crystallogr. D-Biol. Crystallogr. **68**, 1152 (2012) doi:10.1107/S0907444912023475.
54. J. Harms *et al.*, Cell **107**, 679 (2001) doi:10.1016/S0092-8674(01)00546-3.
55. B.T. Wimberly *et al.*, Nature **407**, 327 (2000).
56. S.G.F. Rasmussen *et al.*, Nature **450**, 383 (2007) doi:10.1038/Nature06325.
57. T. Warne *et al.*, Nature **454**, 486 (2008) doi:10.1038/Nature07101.
58. R. Baradaran *et al.*, Nature **494**, 443 (2013) doi:10.1038/Nature11871.
59. A. Amunts *et al.*, J. Biol. Chem. **285**, 3478 (2010) doi:10.1074/jbc.M109.072645.
60. J.E. Burke *et al.*, Science **344**, 1035 (2014) doi:10.1126/science.1253397.
61. J. Fritsch *et al.*, Nature **479**, 249 (2011) doi:10.1038/Nature10505.
62. M. Elias *et al.*, Nature **491**, 134 (2012) doi:10.1038/Nature11517.
63. U.K. Eriksson *et al.*, Science **340**, 1346 (2013) doi:10.1126/science.1234306.
64. A.P. Carter *et al.*, Nature **407**, 340 (2000).